The ASTEC Code: An Algorithm for Solving Thermal-Hydraulic Equations in Complex Geometries

R. D. Lonsdale

United Kingdom Atomic Energy Authority
Dounreay Nuclear Power Development Establishment
Thurso, Caithness, Scotland, KW147TZ, United Kingdom

Received October 12, 1987
Accepted May 19, 1988

Abstract—*By applying a finite volume approach to a finite element mesh, the ASTEC computer code allows three-dimensional incompressible fluid flow and heat transfer in complex geometries to be simulated realistically, without making excessive demands on computing resources. The methods used in the code are described, and examples of the application of the code are presented.*

I. INTRODUCTION

The use of computer codes for modeling three-dimensional, incompressible, single-phase fluid flow and heat transfer is now well established. However, only finite difference/finite volume codes have proved sufficiently economical in their use of computer time and storage to tackle large three-dimensional problems. These codes employ rectilinear meshes, and although coordinate transformations can be used to good effect on some simple problems, accurate representation of the geometry is generally not possible. The finite element method provides the required geometrical flexibility, but it has proved difficult to produce an economical three-dimensional finite element fluid flow code. Standard Galerkin techniques developed for two-dimensional problems may be very expensive when applied without modifications to three dimensions, so that only small meshes can be employed. Gresho et al.[1] and others have modified the finite element method to produce transient three-dimensional codes which, although more expensive than the standard finite difference codes, can be used for realistic applications. However, there are problems with these codes. First, the explicit time differencing introduces a Courant stability restriction on the time-step size, which will make some calculations very expensive. Second, the mesh arrangement is susceptible to spurious pressure checkerboard modes, which can destroy the solution.

This paper describes how a simple finite volume approach has been applied to a finite element mesh, hoping to combine the economy of the former with the geometrical flexibility of the latter in the ASTEC code. Implicit time differencing removes the Courant stability restriction on the time-step size, and, by using a special interpolation procedure on a nonstaggered mesh, pressure checkerboarding is avoided.

A problem to be faced in all fluid flow codes is the representation of the advection terms, since the simplest schemes can produce severe false diffusion in certain circumstances. A skew upwind scheme is employed in ASTEC, which greatly reduces this false diffusion without producing unphysical spatial oscillations in the solution.

The applicability of the code will be discussed, and results from several simulations will be presented.

II. DESCRIPTION

II.A. The Equations

The ASTEC code solves the transient, three-dimensional equations for incompressible fluid flow and heat transfer in a porous medium. The porous medium approximation allows distributed solid structure, such as a rod bundle, which is on too fine a scale for the mesh, to be represented as a continuum with properties of porosity and permeability.[2] A full tensor

representation of the permeability is employed to provide flexibility: For example, a tube bundle can be modeled without requiring the tubes to be aligned with one of the coordinate axes.[3]

By applying the laws of conservation of mass, momentum, and energy to a control volume in the porous medium, we can derive equations for the fluid velocity, pressure, and temperature (see Nomenclature on p. xxx):

$$\int (\mathbf{K}\boldsymbol{u}) \cdot d\boldsymbol{A} = 0 \ , \tag{1}$$

$$\rho \frac{\partial}{\partial t} \int \gamma \boldsymbol{u}\, dV = -\rho \int \boldsymbol{u}(\mathbf{K}\boldsymbol{u}) \cdot d\boldsymbol{A} - \int \gamma \nabla p\, dV + \int \mu[(\mathbf{K}\nabla)\boldsymbol{u}] \cdot d\boldsymbol{A} - \int \gamma \mathbf{R}\boldsymbol{u}\, dV - \rho\beta \boldsymbol{g} \int \gamma T\, dV \ , \tag{2}$$

and

$$\rho c \frac{\partial}{\partial t} \int \gamma T\, dV = -\rho c \int T(\mathbf{K}\boldsymbol{u}) \cdot d\boldsymbol{A} + \int \kappa[(\mathbf{K}\nabla)T] \cdot d\boldsymbol{A} + \int Q\, dV \tag{3}$$

assuming the fluid incompressible.

The volume flux density $\mathbf{K}\boldsymbol{u}$ reduces to the fluid velocity $\boldsymbol{u}$ in open regions (no porous medium), where $\gamma = 1$ and $\mathbf{K}$ is the identity matrix $\mathbf{I}$.

Equation (1) expresses the fact that there should be no net gain/loss of fluid in the control volume.

The left side of Eq. (2) is the rate of gain of momentum within the fluid in the control volume, with the terms on the right side representing, respectively, advection through the control volume surface, the acceleration due to a pressure gradient, diffusion through the surface, drag due to the solid structure forming the porous medium, and buoyancy forces (using the Boussinesq approximation).

Equation (3) balances the rate of gain of heat in the fluid within the control volume, against advection and diffusion through the surface of the control volume, and the heat gained from the solid structure of the porous medium.

With $\mathbf{K} = \mathbf{I}$, $\gamma = 1$, $\mathbf{R} = 0$, $Q = 0$, these equations reduce those for laminar flow of an incompressible fluid, with no porous medium. For turbulent flow in such open regions, ASTEC employs a two equation turbulence transport model, namely, the k-ϵ model, with wall functions for modeling solid boundaries.[4] When using this turbulence model, transport equations for k and ϵ must be solved in addition to Eqs. (1), (2), and (3).

II.B. The Mesh

We wish to construct, and then solve, equations for the variables $\boldsymbol{u}$, p, T, k, and ϵ at a finite number of nodal positions. Each node must be surrounded by a control volume, to which we can apply an approximation of Eqs. (1), (2), and (3) in order to provide equations for the discrete nodal values of the variables. Thus, our first step is to construct these nodal control volumes.

Let us consider the two-dimensional situation. We divide the region we wish to model into arbitrary quadrilaterals, called elements, the corners of which will be our nodal positions (Fig. 1). Joining the midpoints of opposite sides in every element defines a control volume around each node. Moving to three dimensions, we split our region into eight-node blocks. Within each block (element) we specify points at the midpoint of each edge, at the center of gravity of the four nodes on each face, and at the center of gravity of the eight nodes forming the element (this last point is denoted by an ellipse containing a cross in Fig. 2). These points are joined, as illustrated in Fig. 2, to construct a control surface around each node, which encloses the nodal control volume. The four points that define each face of the control surface need not be coplanar; the face is constructed from two triangles

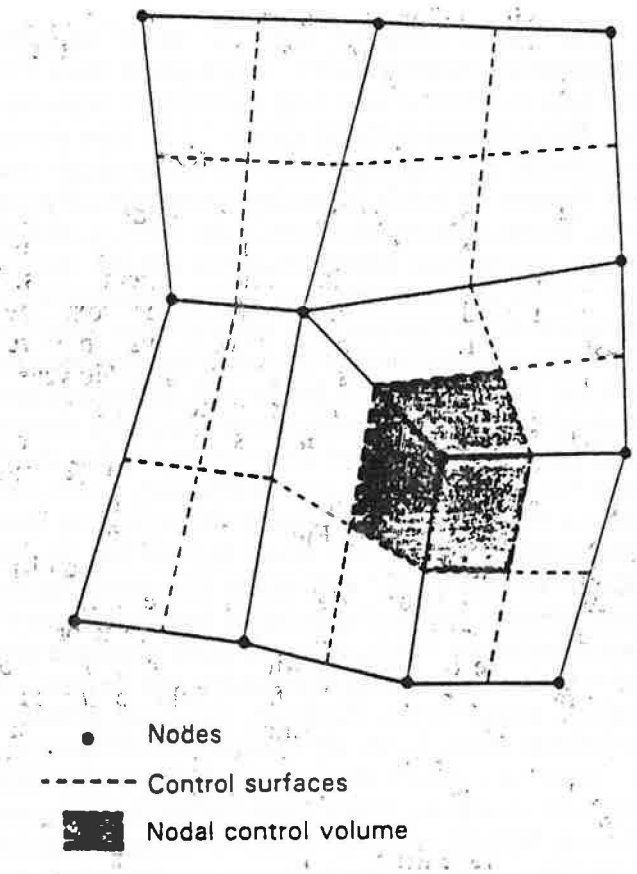

Fig. 1. A two-dimensional mesh of quadrilateral elements.

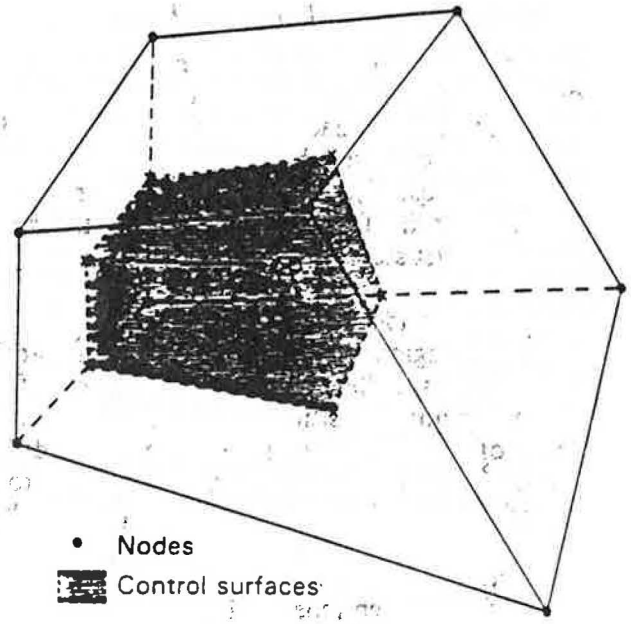

Fig. 2. An eight-node element used for three-dimensional meshes.

when the surface is not planar. Although each element must have eight nodes, note that there is no restriction regarding the number of elements to which a particular node belongs.

Having defined the control volumes, we must construct a discrete representation for each of the terms in Eqs. (1), (2), and (3).

II.C. Discretization

All variables are stored at the nodes. The difference scheme is implicit in time, i.e., latest values are used for all variables in the nontransient terms. Volume integrals in Eqs. (2) and (3) are approximated by assuming that the mean value of the variable over the control volume equals the nodal value. However, the pressure gradient term is converted to a surface integral of pressure using Gauss's divergence theorem.

Now the surface integrals in Eqs. (1), (2), and (3) are evaluated by summing over the faces of the control surface shown in Fig. 2. On each face, we must approximate the pressure, and advective and diffusive fluxes, in terms of nodal values of the variables. Then the scalar product of this flux with the vector area $\boldsymbol{dA}$ of the face provides us with the contribution to the surface integral from this face of the control surface.

For the pressure, we simply assume the pressure on the face to be the mean of the pressures at the two nodes whose control volumes are separated by the face.

Each face lies within an element, and only nodes belonging to that element are used when calculating the flux through the face. For the diffusive flux, the gradient of the variable is estimated from the nodal values around the element containing that face. When calculating the advective flux through a face, central differencing is used for low mesh Peclet numbers (<2), with a proportion of upwinding employed when mesh Peclet numbers exceed two. A form of streamline upwinding is used to reduce false diffusion when the flow lies at an angle to the mesh. The flow through the face is estimated from the adjacent nodal velocities by employing the interpolation procedure of Rhie and Chow.[5] This allows both pressures and velocity components to be stored at the nodes, with mass conservation satisfied in the nodal control volumes and with no pressure checkerboarding problems.

The procedure for solving the discrete equations is iterative and based on the SIMPLE method.[6] Each iteration consists of one sweep through the velocity, temperature, and turbulence equations followed by the calculation of pressure and velocity corrections required to satisfy mass conservation. A preconditioned conjugate gradient algorithm is used to calculate these pressure corrections. Iterations are performed until changes in the variables are small enough to satisfy prescribed convergence criteria, at which stage we move on to the next time step in a transient calculation, or finish in the case of a steady-state calculation.

III. APPLICATIONS

III.A. Discussion

The ASTEC code combines many desirable features, making it suitable for a variety of industrial applications.

The finite element mesh allows great geometrical flexibility, so that complex geometries can be modeled with relative ease. Distributed solid structure, such as a rod bundle, can be represented by means of the porous medium approximation; a tensor permeability is employed to allow greater flexibility.

The transient equations are solved using an implicit differencing scheme, so avoiding Courant stability restrictions on the time-step size. A hybrid skew upwinding scheme greatly reduces the false diffusion arising from the advective terms.

A two equation turbulence transport model (including buoyancy effects), which uses wall functions, is available for modeling turbulent flow in open regions.

The computer storage requirements are proportional to the mesh size, with a mesh of 8000 nodes requiring 1.7 megawords of memory.

To give some idea of the speed, the run time required for a particular problem will be given. This problem will be discussed in Sec. III.D and involves calculating steady isothermal turbulent flow using the k-ϵ model on a mesh of ~8000 nodes. A converged solution was obtained in 25 min on a CRAY X-MP

machine, which is not significantly slower than other three-dimensional finite volume codes, which may be restricted to rectilinear or cylindrical polar meshes.

The ASTEC code was originally developed to simulate natural convection in the primary tank of pool-type liquid-metal fast breeder reactors—a problem that demands a three-dimensional code capable of representing a highly complex geometry with great variations in length scale. Work has started on applying the code to this difficult problem.

III.B. Benchmark Test

Before we can place any confidence in our computational results, it is necessary to provide some validation of the code. Simple tests were carried out during the development stage, but to ensure that the differencing scheme produces acceptable accuracy, ASTEC has been applied to a test problem involving two-dimensional laminar flow in a smoothly expanding plane channel for two values of the Reynolds number (Re = 10 and Re = 100) (Ref. 7). Figure 3 shows the mesh used for the low Reynolds number case.

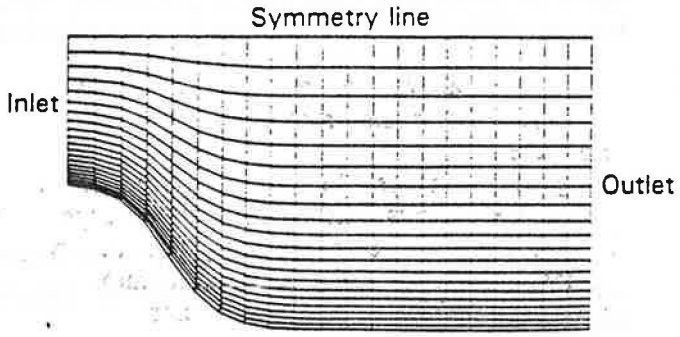

Fig. 3. ASTEC mesh for the two-dimensional benchmark problem.

Mesh-independent benchmark solutions, for both values of the Reynolds number, were obtained by Cliffe et al.[8] using a finite element code with a very fine mesh. The ASTEC results for wall vorticity and wall pressure on a 21 × 21 mesh are compared with this benchmark solution in Fig. 4, for the Re = 100 case, with the crosses representing the benchmark solution. Agreement is generally very good, considering the coarseness of the mesh, with similarly satisfactory results being observed for Re = 10. There is a singularity in the pressure solution at the inlet, which is responsible for the discrepancy in this region: The same difficulty was encountered with other codes applied to this problem.[7]

The successful results from this benchmark test allow us to have some confidence in the differencing scheme.

III.C. The SONACO Experiment

The SONACO project aims to experimentally investigate the free convection cooling of fast reactor fuel pin assemblies that are blocked at the inlet or outlet. A 37-pin electrically heated bundle is immersed in liquid sodium within a hexagonal wrapper, and a flow of sodium outside this wrapper is used to take away the heat (in the radial cooling mode). Since no flow is allowed through the test section within the wrapper, natural convection currents are set up that enhance heat transfer from the pin bundle to the wrapper. Reference 9 contains details of the design of the experiment.

The ASTEC code has been applied to one of the SONACO experiments. Figure 5 shows the mesh of 3465 elements, representing a 30-deg sector of the hexagonal test section, which is used for simulating radially symmetric heating modes. The porous medium approximation is employed to represent the bundle,

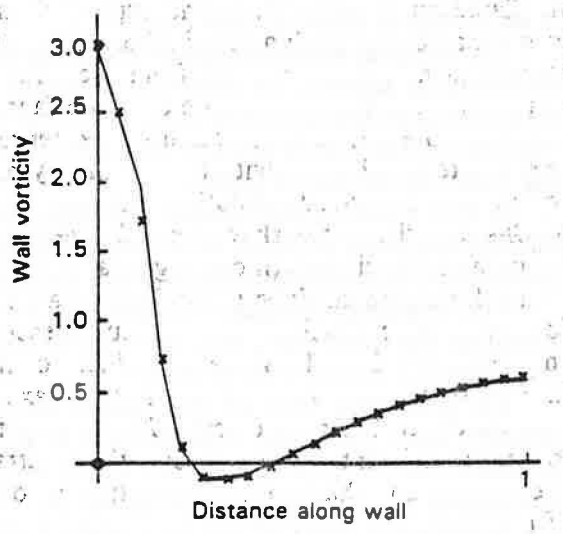

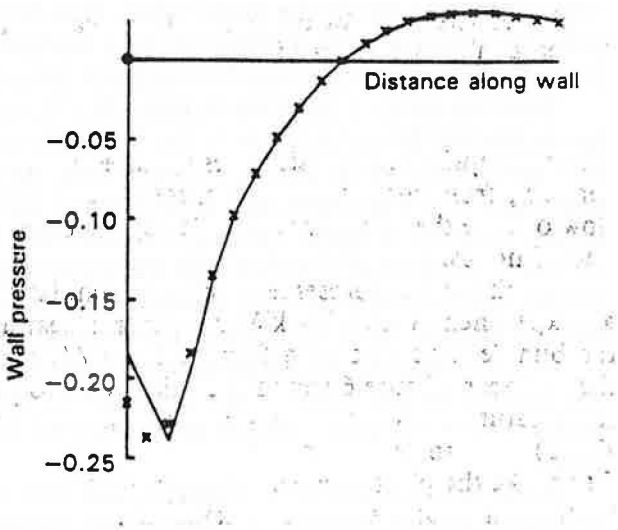

Fig. 4. Comparison between ASTEC predictions and the benchmark solution (the crosses).

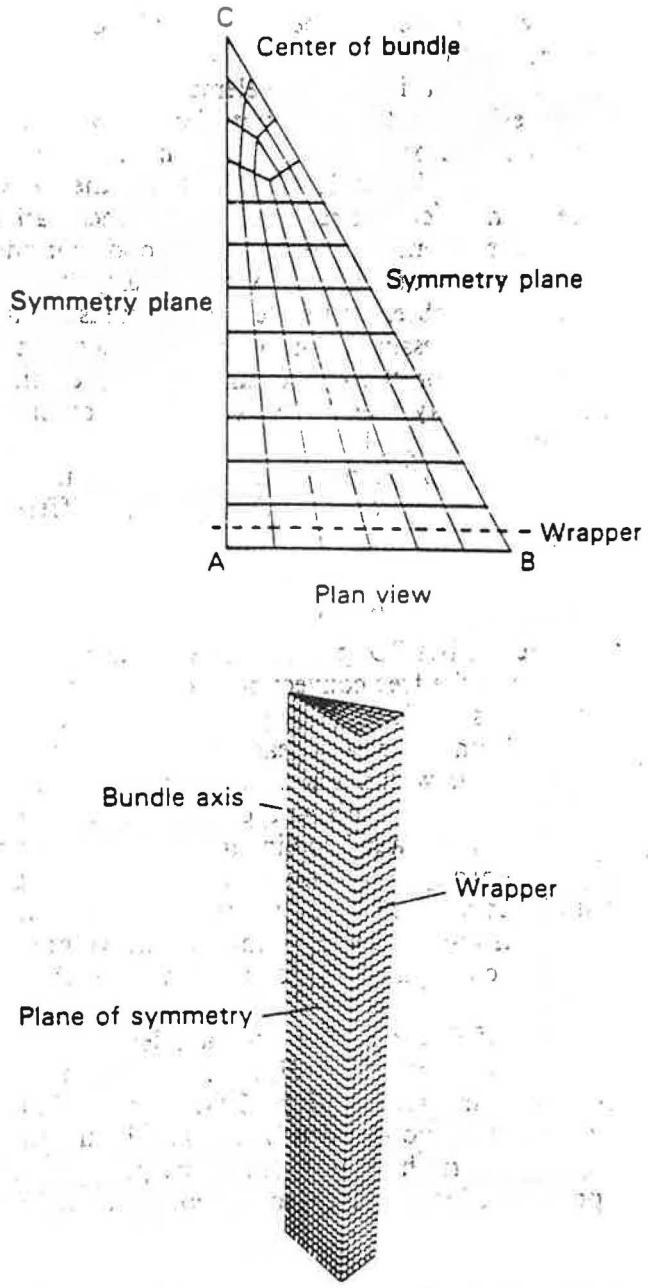

Fig. 5. The mesh for the SONACO simulation, compressed axially by a factor of 5.

with appropriate flow resistances specified to account for drag from the bundle and spacer grids. Cooling flow outside the wrapper is modeled by the outermost line of nodes.

Results will be presented from the simulation of an experiment with 29.4 kW of uniform heating in the bundle, and a cooling flow of 0.247 ℓ/s outside the wrapper. Figure 6 shows the velocity vectors and temperature contours in the symmetry plane C-A (see Fig. 5), with the axial scale compressed by a factor of 5 to make the plots clearer. As expected there is flow up the center of the bundle, extending into a plenum above the bundle, and flow down by the wrapper, all

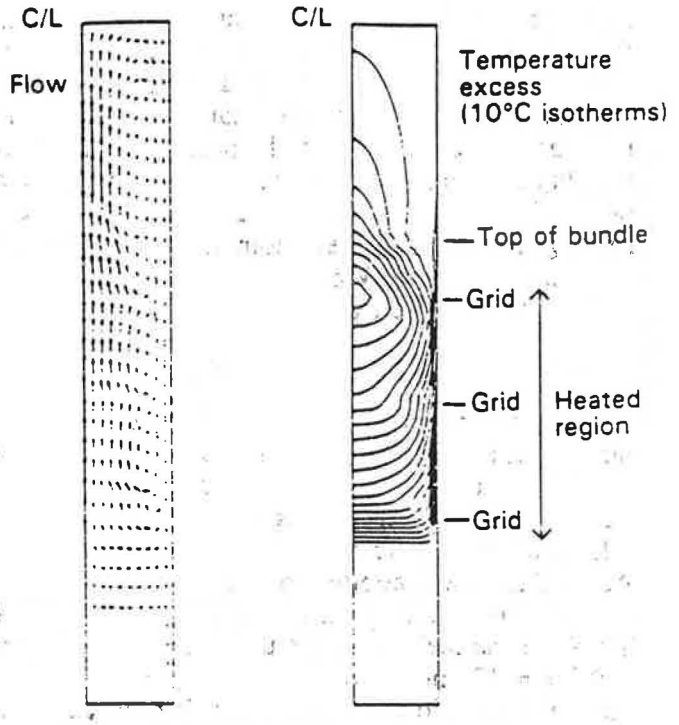

Fig. 6. Flow vectors and isotherms on SONACO symmetry plane.

driven by buoyancy. The maximum temperature occurs at the top of the heated region on the central axis of the bundle.

Figure 7 compares the ASTEC prediction for the temperatures on this central axis with the experimental results.[10] The agreement is very satisfactory. Unfortunately, there are no reliable velocity measurements currently available from this particular experiment.

III.D. Turbulent Ventilated Box

To demonstrate the use of the turbulence model in ASTEC, calculations were performed to simulate a ventilated box experiment.[11] This experiment involved turbulent flow through a cuboidal box (Fig. 8) with a square entrance in the center of one face and a larger square exit in the center of the opposite face.

Using the mesh illustrated in Fig. 9, representing one-quarter of the box with two symmetry planes, a converged steady-state solution was obtained with the k-ϵ model and the skew upwind advection treatment on all variables (including k and ϵ) to minimize false diffusion. Experimental results are available for the mean axial velocity and the turbulence kinetic energy k, at points along the central axis of the box. In Fig. 10, we show our predictions for the axial velocity, and the turbulence velocity $(2k/3)^{1/2}$, compared to the experimental values along this central axis. Clearly, the code has overpredicted the rate of spread of the jet.

Previous experience with other codes in applying

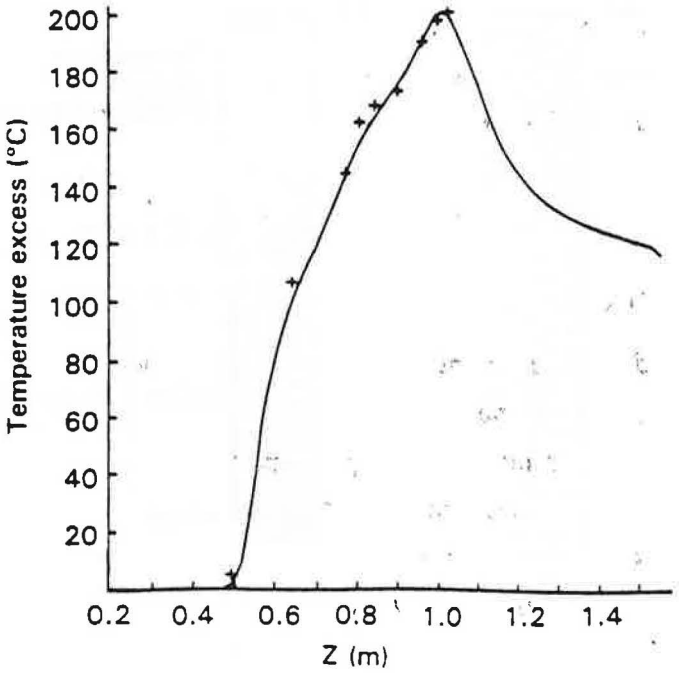

Fig. 7. Comparison between the predicted axial temperature variation and experimental results (the crosses) from SONACO.

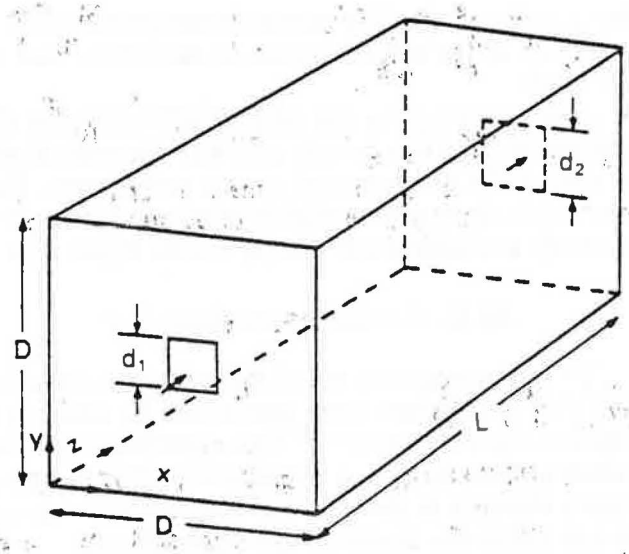

Fig. 8. Geometrical configuration of the ventilated box experiment. Here, $D = 100$ mm, $L/D = 3.0$, two symmetry planes; $d_1/D = 0.1$, $d_2/D = 0.2$, mean inlet velocity = 18.5 ms^{-1}.

the k-ϵ model to round jets has implied that the constant c_1 in the ϵ equation should be changed from its standard value, $c_1 = 1.44$, to $c_1 = 1.6$ for this situation.[12] Using this new value for c_1, our results slightly underpredict the rate of spread of the jet (Fig. 11).

Note that broadly similar results have been obtained by workers using other codes on this problem.[11,12]

The computational mesh is probably too coarse,

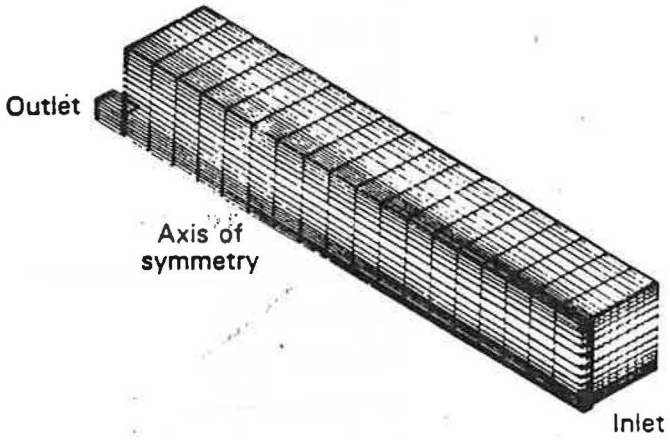

Fig. 9. Mesh for the ventilated box.

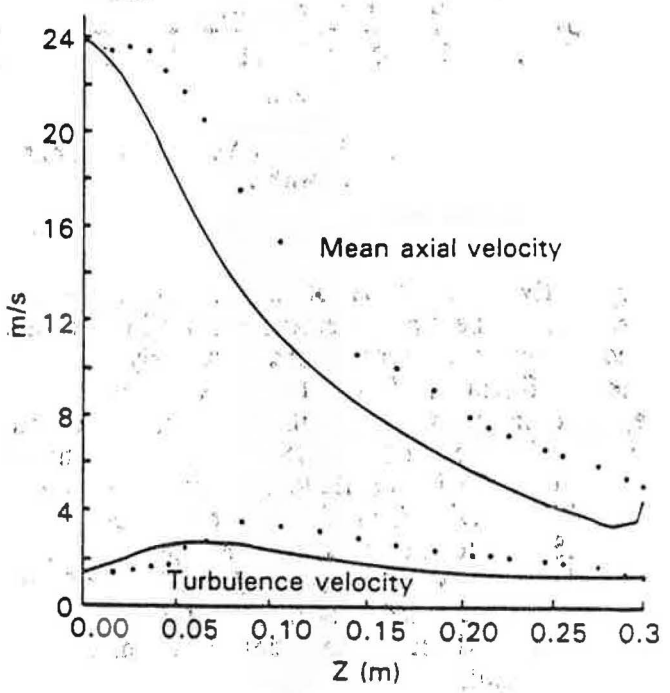

Fig. 10. Comparison between ASTEC predictions and experimental results (dots) for mean axial and turbulence velocities on the symmetry axis, with $c_1 = 1.44$.

especially around the inlet, for us to have much confidence in these results, and so this cannot be viewed as a rigorous test of the k-ϵ model. However, the availability of larger computers in the near future should allow a much finer mesh to be used near the inlet, hopefully improving the reliability of the results.

IV. CONCLUSION

Finite volume methods have been applied on a finite element mesh to produce ASTEC: A fluid flow code with great geometrical flexibility, which is not

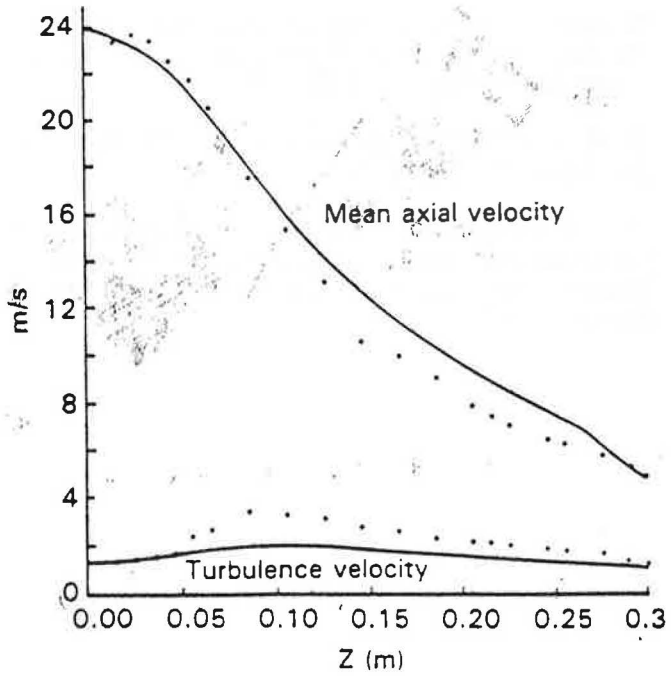

Fig. 11. Comparison between ASTEC predictions and experimental results (dots), with $c_1 = 1.6$.

prohibitively expensive on large, three-dimensional problems. The finite element mesh allows complex geometries to be reproduced accurately, with local mesh refinement if required. The porous medium approximation, with the full tensor representation of permeability, can be used to represent any fine-scale solid structure in the flow. A turbulence transport model is available for turbulent flow in open regions. The ASTEC code also uses a skew upwind treatment for advection, which greatly reduces false diffusion.

Results presented in Sec. III demonstrate the ability of the code to model complex geometries with accurate results.

The ASTEC code should prove a valuable tool for performing three-dimensional thermal-hydraulic calculations in complex geometries.

NOMENCLATURE

c_p = fluid specific heat capacity

$d\mathbf{A}$ = element of control surface area

dV = element of control volume

g = gravitational acceleration

$\mathbf{K}$ = permeability tensor

k = turbulence kinetic energy density

p = pressure

Q = heat source density

$\mathbf{R}$ = resistivity tensor

Re = Reynolds number

T = fluid temperature

t = time

$\boldsymbol{u}$ = fluid velocity

Greek

β = coefficient of volumetric expansivity

γ = volume porosity

ϵ = turbulence energy dissipation rate

κ = thermal conductivity

μ = dynamic viscosity

ρ = density

ACKNOWLEDGMENTS

I would like to thank A. D. Burns, I. P. Jones, and J. R. Kightley at Harwell, and P. T. Dutton, B. R. MacGregor, and R. Webster at Dounreay, for much useful advice and discussion. Special thanks are due to B. R. MacGregor, whose work on the LUNE code provided a basis for the development of ASTEC.

For making the SONACO experimental results available, I am indebted to the Federal Institute for Reactor Research, Würenlingen.

I would also like to thank the director at Dounreay, C. W. Blumfield, for permission to publish this paper.

REFERENCES

1. P. M. GRESHO et al., *Int. J. Numerical Methods in Fluids*, **4**, 557 (1984).

2. S. WHITAKER, *Ind. Eng. Chem.*, **61**, *12*, 14 (1969).

3. R. WEBSTER, "A Three-Dimensional Thermal Hydraulic Analysis of the PFR Steam Generators," presented at 1st U.K. Natl. Conf. Heat Transfer, Leeds, U.K., July 3–5, 1984.

4. F. F. CHEN et al., "Turbulence Modelling in the COMMIX Computer Code," NUREG/CR-3504, ANL-83-65, Argonne National Laboratory (1984).

5. C. M. RHIE and W. L. CHOW, *AIAA J.*, **21**, *11* (1983).

6. S. V. PATANKAR, *Numerical Heat Transfer and Fluid Flow*, Hemisphere Publishing Corporation, New York (1980).

7. M. NAPOLITANO and P. ORLANDI, *Int. J. Numerical Methods in Fluids*, **5**, 667 (1985).

8. K. A. CLIFFE et al., "Finite Element Solutions for Flow in a Symmetric Channel with a Smooth Expansion" AERE-R-10608, U.K. Atomic Energy Authority (1982).

9. T. V. DURY, "SONACO Liquid Sodium Experiments—Final Design Specification: Phase 1—Natural Convection," TM-23-83-17, Institute for Reactor Research (1983).

10. T. V. DURY et al., "Radial Heat Removal from the SONACO Sodium-Cooled Rod Bundle Compared with Bacchus-T and INCA Computer Prediction," presented at 3rd Int. Conf. Reactor Thermal Hydraulics, Newport, Rhode Island, October 15–18, 1985.

11. B. H. HJERTAGER and B. F. MAGNUSSEN, *Comput. Fluids*, **9**, 395 (1981).

12. I. P. JONES et al., "FLOW3D, A Computer Code for the Prediction of Laminar and Turbulent Flow, and Heat Transfer: Release 1," AERE-R-11825, U.K. Atomic Energy Authority (1985).